Structure of Three Class I Human Alcohol Dehydrogenases Complexed with Isoenzyme Specific Formamide Inhibitors[†,‡]

Brian J. Gibbons and Thomas D. Hurley*

Department of Biochemistry and Molecular Biology, Indiana University School of Medicine, 635 Barnhill Drive, Room MS 4017, Indianapolis, Indiana 46202-5122

Received May 27, 2004; Revised Manuscript Received July 30, 2004

ABSTRACT: Formamides are aldehyde analogues that have demonstrated potent and selective inhibition of human alcohol dehydrogenase isoenzymes. The $\alpha\alpha$, $\beta_1\beta_1$, $\gamma_2\gamma_2$, and $\sigma\sigma$ isoforms have all been found to be strongly inhibited by substituted formamides. In this paper, the structure of the $\alpha\alpha$ isoform of human alcohol dehydrogenase complexed with *N*-cyclopentyl-*N*-cyclobutylformamide was determined by X-ray crystallography to 2.5 Å resolution, the $\beta_1\beta_1$ isoform of human alcohol dehydrogenase complexed with *N*-benzylformamide and with *N*-heptylformamide was determined to 1.6 and 1.65 Å resolution, respectively, and the structure of the $\gamma_2\gamma_2$ isoform complexed with *N*-1-methylheptylformamide was determined to 1.45 Å resolution. These structures provide the first substrate-level view of the local structural differences that give rise to the individual substrate preferences shown by these highly related isoenzymes. Consistent with previous work, the carbonyl oxygen of the inhibitors interacts directly with the catalytic zinc and the hydroxyl group of Thr48 (Ser48 for $\gamma_2\gamma_2$) of the enzyme. The benzene ring of *N*-benzylformamide and the carbon chains of *N*-heptylformamide and *N*-1-methylheptylformamide interact with the sides of the hydrophobic substrate pocket whose size and shape is dictated by residue exchanges between the $\beta_1\beta_1$ and $\gamma_2\gamma_2$ isoenzymes. In particular, the exchange of Ser for Thr at position 48 and the exchange of Val for Leu at position 141 in the $\gamma_2\gamma_2$ isoenzyme create an environment with stereoselectivity for the R-enantiomer of the branched *N*-1-methylheptylformamide inhibitor in this isoenzyme. The primary feature of the $\alpha\alpha$ isoform is the Ala for Phe93 exchange that enlarges the active site near the catalytic zinc and creates the specificity for the branched *N*-cyclopentyl-*N*-cyclobutylformamide inhibitor, which shows the greatest selectivity for this unique isoenzyme of any of the formamide inhibitors.

Excess ethanol consumption is believed to contribute to many pathologic conditions including malnutrition, heart disease, liver disease, and cancer (*1*). The severity of these conditions depends on the amount and the time course of ethanol consumed and upon the ability of the human body to metabolize and eliminate ethanol. In humans, there are several systems that contribute to ethanol metabolism including first-pass metabolism in the stomach, the microsomal ethanol oxidizing system (MEOS), catalase, and the alcohol dehydrogenase (ADH) enzymes (*1*). The relative contribution of each of these systems toward the oxidation of ethanol and other dietary and biogenic alcohols and aldehydes is not fully understood (*1*). It is currently believed that the ADH isoenzymes provide the major pathway for the metabolism of consumed ethanol as well as other alcohols and aldehydes that are biologically important (*2*). Since the ADH enzymes contribute significantly to the metabolism of many different compounds, it is likely that consumption of excess ethanol perturbs many pathways by competing with the physiologic substrates. For example, inhibition of ADH-mediated retinoic

acid synthesis by consumed ethanol may contribute to the abnormalities associated with fetal alcohol syndrome (*3*). It is, therefore, important to develop different methodologies to study the role of human ADH enzymes in alcohol and aldehyde metabolism.
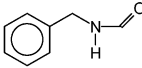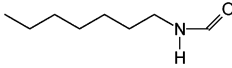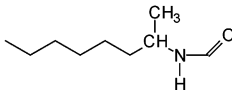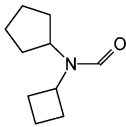
The zinc-dependent medium chain alcohol dehydrogenases are cytosolic, dimeric isoenzymes that catalyze the NAD-(H)-dependent, reversible oxidation of alcohols to their corresponding aldehydes or ketones (*4*). Seven zinc-dependent ADH genes (*ADH1−ADH7)* have been identified in humans (*5*). The $\alpha\alpha$, $\beta_1\beta_1$, $\gamma_1\gamma_1$, $\pi\pi$, and $\chi\chi$ isoenzymes are encoded by the *ADH1A*, *ADH1B*, *ADH1C*, *ADH4*, and *ADH5* genes, respectively (*6*). No human protein product has yet been identified in vivo for the *ADH6* gene (*6*). The *ADH7* gene encodes the $\sigma\sigma$ isoenzyme (*5*). Functional polymorphisms have been identified at the *ADH1B* ($\beta_1\beta_1$, $\beta_2\beta_2$, and $\beta_3\beta_3$) and *ADH1C* ($\gamma_1\gamma_1$, and $\gamma_2\gamma_2$) loci (*5*). The different human isoenzymes exhibit divergent enzymatic characteristics with respect to their turnover rate and catalytic efficiency toward ethanol. A classification scheme has been devised for the ADH isoenzymes based on their amino acid sequences and enzymatic characteristics (*6*). The class I, II, and III ADH isoenzymes are all expressed primarily in the liver, while the class IV ADH is expressed primarily in epithelial tissue, such as stomach mucosa (*7*). There is approximately 93% sequence identity between the class I

‡ The structure factors and derived atomic coordinates have been deposited with the Protein Data Bank under codes 1U3T, 1U3U, 1U3V, and 1U3W.

* To whom correspondence should be addressed. Fax: (317) 274-4686. Phone: (317) 278-2008. E-mail: thurley@iupui.edu.

Table 1: Inhibition Constants for Substituted Formamides[a] (μM)

Formamide Inhibitor	ADH Isoenzyme				
	$\alpha\alpha$	$\beta_1\beta_1$	$\gamma_2\gamma_2$	$\pi\pi$	$\sigma\sigma$
N-benzylformamide	31	*0.33*	**4.9**	110	11
N-heptylformamide	3.6	*0.33*	12	11	*0.74*
(R,S)-N-1-methylheptylformamide	7.0	1.7	*0.41*	40	100
N-cyclopentyl-N-cyclobutylformamide	*0.36*	10000	47	360	1100

[a] Data extracted from ref *13*.

ADH isoenzymes (*ADH1A*, *ADH1B*, and *ADH1C* gene products), and they have been shown to form both homo- and heterodimers (e.g., $\alpha\beta_1$) (*5, 8*). Although the overall sequence identity among the Class I ADH isoenzymes is high, the identity between the active sites is lower; ranging between 50 and 70% sequence identity in pairwise comparisons (*9*). The differences between the active sites are substantial enough that selective inhibitor design is feasible. In contrast to these within class properties, the other classes of ADH exhibit roughly 60% sequence identity with the class I ADH isoenzymes and have only been found as homodimers (*2*).

Over the years, in vitro studies of the human isoenzymes have provided valuable information but have not established unambiguous roles for the human ADH isoenzymes in vivo. Recent in vivo studies in ADH null mutant mice support some of the in vitro findings (*10*) but cannot address the issue of the human class I ADH isoenzymes since mice possess only one isoenzyme in this class, whereas humans have three. Nor can this type of study be applied to the class II or V ADH enzymes. The mouse class II ADH has very different properties than the orthologous human form (*11*), and a class V ADH has not been identified in mice (*6*). One potential approach to studying human ADH isoenzymes in vivo would be to measure substrate metabolism in the presence of isoenzyme specific inhibitors.

Several types of ADH inhibitors have been identified. Most, including 4-methylpyrazole, are not useful for such studies because they do not selectively inhibit specific ADH isoenzymes (*12*). To date, the most promising class of inhibitors for studying ADH function are formamides (*13*). Formamides are unreactive aldehyde analogues that dem-

onstrate potent and selective inhibition of human ADH isoenzymes. The $\alpha\alpha$, $\beta\beta$, $\gamma\gamma$, and $\sigma\sigma$ isoforms of ADH have all been found to be strongly inhibited (sub-micromolar K_i values) by variously substituted formamides (Table 1). The formamides bind to the ADH−NADH complex and are, therefore, uncompetitive against alcohols and competitive against aldehydes or ketones (*13*). Inhibitors of this class have been shown to decrease ethanol elimination in vivo and could prove to be effective in blocking production of toxic alcohol metabolites, such as formic acid and glycolic acid, which are produced by the ADH-facilitated oxidation of methanol and ethylene glycol, respectively (*14*).

The structural dimensions and properties of the active sites of the human $\alpha\alpha$, $\beta_1\beta_1$, $\gamma_2\gamma_2$, and $\sigma\sigma$ ADH isoenzymes vary considerably due to amino acid substitutions within their substrate binding sites (*9, 15*). The aim of this study was to obtain detailed three-dimensional structural information about the binding of isoenzyme-specific formamides to human ADH isoenzymes. We present here the structures of the three class I ADH isoforms complexed with their respectively most potent formamide inhibitors. These structures provide the first substrate-level view of the structural differences that underlie the characteristic substrate specificities of each individual isoenzyme. These inhibitors could find use in studies designed to assess the contribution of a particular ADH isoenzyme toward the metabolism of a particular substrate or may be useful for identification of physiologic substrates for each isoenzyme.

EXPERIMENTAL PROCEDURES

Enzyme Expression, Purification, and Crystallization. The human $\alpha\alpha$, $\beta_1\beta_1$, and $\gamma_2\gamma_2$ ADH isoenzymes were expressed

Table 2: Data Collection and Refinement Statistics

	$\beta_1\beta_1$−BF complex	$\beta_1\beta_1$−HF complex	$\alpha\alpha$−CPCB complex	$\gamma_2\gamma_2$−MHF complex
	Diffraction Data Statistics			
space group	*P*1	*P*1	*P*2$_1$	*P*2$_1$
cell dimensions (*a, b, c*, in Å)	44.8, 52.5, 90.1	44.3, 52.8, 90.4	56.0, 71.5, 92.8	55.4, 67.1, 92.7
cell angles (α, β, γ, in deg)	79.8, 89.7, 69.0	79.6, 89.4, 68.6	90, 102.8, 90	90, 103.8, 90
resolution range (Å)	30−1.6	30−1.65	30−2.49	29−1.45
total observations	237103	238652	38928	423198
unique reflections	88870	80448	23930	116320
completeness[a] (%)	90.2 (78.2)	89.4 (69.8)	90.0 (78.6)	99.6 (99.0)
R_{merge}[a] (%)	4.6 (17.2)	3.7 (15.1)	7.5 (36.2)	5.2 (43.2)
I/σ_I[a]	20.9 (6.6)	29.9 (7.6)	11.3 (3.0)	17.2 (3.1)
refinement statistics				
test set size (% of total)	5[b]	5[b]	5	5
R_{work}/R_{free}	0.169/0.190	0.165/0.185	0.202/0.232	0.184/0.211
average *B*-value	19.6	18.0	21.6	21.0
r.m.s. deviation from ideal bond lengths (Å)	0.009	0.010	0.010	0.020
r.m.s. deviation from ideal bond angles (deg)	2.23	1.74	2.06	1.84

[a] The corresponding statistics for the high-resolution shells (10 equal bins) within each data set are given in parentheses. [b] These structures were refined using identically flagged sets of R_{free} reflections.

and purified using published procedures (*9*). The purity of each alcohol dehydrogenase isoenzyme was monitored and confirmed using SDS−PAGE and ADH activity assays as previously described (*9*). All crystals were grown using the sitting drop vapor diffusion method at 4 °C. $\alpha\alpha$ crystals were grown at 6.5 mg/mL enzyme, 3 mM NAD$^+$, 100 mM Na-ACES, pH 6.0−6.1, and 13−15% PEG 6000. $\beta_1\beta_1$ crystals were grown at 15 mg/mL enzyme, 2 mM NAD$^+$, 50 mM sodium phosphate, pH 7.5, and 11.5−13% PEG 8000. $\gamma_2\gamma_2$ crystals were grown at 10 mg/mL enzyme, 4 mM NAD$^+$, 50 mM Tris-HCl, pH 9.0, and 17−19% PEG 6000.

In all cases, the isoenzymes were crystallized as binary complexes with the cofactor NAD$^+$. The inhibitors were then soaked into the crystals by transferring the crystals into solutions of mother liquor containing 1 mM appropriate inhibitor and 1 mM NADH, substituting for NAD$^+$. The inhibitors were obtained from Dr. Bryce Plapp (University of Iowa) in lyophilized form and were reconstituted to 10 mM with ultrafiltered, deionized water. Following soaking, the crystals were flash-frozen to −165 °C and then examined for their ability to diffract X-rays to high resolution using the crystallographic equipment associated with the Center for Structural Biology located in the Department of Biochemistry and Molecular Biology.

Data Collection. The $\beta_1\beta_1$ and $\alpha\alpha$ diffraction data were collected on the Rigaku H2R rotating anode X-ray generator equipped with a Rigaku RAXIS IIC image plate area detector associated with the Center for Structural Biology. The $\gamma_2\gamma_2$ diffraction data were obtained using synchrotron radiation on equipment associated with Beamline X12B at the National Synchrotron Light Source located at the Brookhaven National Laboratories. All the diffraction data were indexed, integrated, and scaled using the HKL (v1.97.2) suite of programs (*16*). The raw intensity data were subsequently converted to their individual structure−factor components using the program TRUNCATE as implemented in the CCP4 suite of programs (*17*).

Structure Solution. The structures of the human $\alpha\alpha$, $\beta_1\beta_1$, and $\gamma_2\gamma_2$ isoenzymes complexed with their selective formamide inhibitors were solved using the program AMORE (*18*) for molecular replacement and the existing coordinates for each isoenzyme−1HSO, 1HSZ, and 1HT0, respectively. Prior to use for molecular replacement, all ligands and solvent

molecules, with the exception of the bound zinc ions, were removed from each coordinate file. Following successful identification of each orientation solution, the structures were refined using CNS (*19*) ($\alpha\alpha$ and $\beta_1\beta_1$) or CNS and Refmac5 (*20*) ($\gamma_2\gamma_2$). Only for the refinement of the $\alpha\alpha$ isoenzyme were bond and angle restraints applied to maintain the metal−ligand geometries of the active site and structural zinc centers. Each structure was refined using iterative cycles of restrained automated refinement of the atomic positions and individual restrained isotropic temperature factor refinement utilizing a maximum-likelihood target function, followed by manual inspection of the resulting structures using σA, figure-of-merit-weighted electron density maps in the program O (*21*). Parameters for the restrained refinement of each formamide inhibitor were developed using XPLO2D routine associated with the program O combined with manual adjustment of the dihedral and improper restraints. No restraint was utilized between the catalytic zinc atoms and the carbonyl oxygen atom of each inhibitor.

RESULTS

The structure of the human $\alpha\alpha$ ADH isoenzyme complexed with *N*-cyclopentyl-*N*-cyclobutylformamide (**CPCB**) was solved to 2.49 Å, the structure of the human $\beta_1\beta_1$ ADH isoenzyme complexed with *N*-benzylformamide (**BF**) and with *N*-heptylformamide (**HF**) was solved to 1.60 and 1.65 Å, respectively, and the $\gamma_2\gamma_2$ isoform complexed with *N*-1-methylheptylformamide (**MHF**) was solved to 1.45 Å. All structures were refined using the programs CNS and/or Refmac5. A summary of the data collection and structure refinement statistics is presented in Table 2.

The $\alpha\alpha$, $\beta_1\beta_1$, and $\gamma_2\gamma_2$ crystals all have a dimer comprising the asymmetric unit. The $\alpha\alpha$, $\beta_1\beta_1$, and $\gamma_2\gamma_2$ isoenzymes share 93% sequence identity, and their overall structures are virtually identical. Pairwise coordinate alignments using the Cα atoms of individual subunits show between 0.3 and 0.4 Å root-mean-square deviations in atomic positions not involved in lattice contacts. As previously described, there is a slightly more closed conformation of the catalytic domain, relative to the coenzyme domain, in the $\alpha\alpha$ isoenzyme that slightly narrows the entrance to the substrate-binding site but otherwise has minimal impact on the
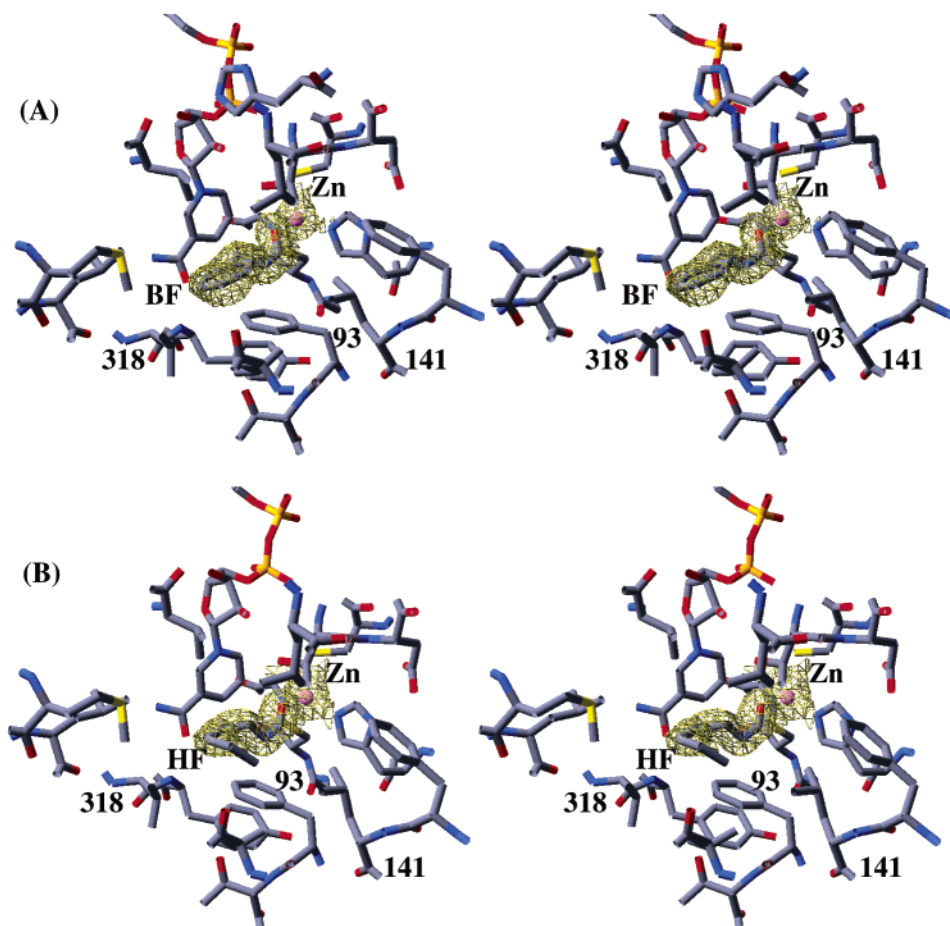
FIGURE 1: Electron density for the bound benzylformamide (A) and bound heptylformamide (B) in the substrate-binding site of human $\beta_1\beta_1$ alcohol dehydrogenase. Figures 2–4 were produced using the program SPDB Viewer (*28*) and rendered using the program POV-RAY.

structure–activity relationships of substrate binding to this isoenzyme (*9*). Consequently, the structures of the respective substrate-binding pockets of these isoenzymes differ primarily as a result of the amino acid substitutions that occur within this binding pocket.

The interactions between the bound formamides and the catalytic zinc, position 48, and the nicotinamide rings are all similar to that observed when bound to equine liver alcohol dehydrogenase (*14, 22*). In all cases, the carbonyl oxygen of the inhibitor coordinates directly to the catalytic zinc atom at distances between 2.1 and 2.4 Å and forms a hydrogen bond with the hydroxyl group of Thr48 in the enzymes (Ser48 in $\gamma_2\gamma_2$). Each inhibitor presents its re-face toward the nicotinamide ring of the bound coenzyme. The C4 atoms of the nicotinamide rings and the carbonyl carbon atoms of the inhibitors are an average of 3.8, 3.9, and 3.4 Å from each other in the $\alpha\alpha$, $\beta_1\beta_1$, and $\gamma_2\gamma_2$ structures, respectively. However, only in the $\alpha\alpha$ structure is the angular relationship between the two sp²-hybridized carbon centers optimal for hydride transfer. The benzyl ring of the inhibitor **BF** is located in the entrance pocket of the $\beta_1\beta_1$ active site where it interacts with the hydrophobic residues that project from its surface (Figure 1A). In the two $\beta_1\beta_1$ structures, the same residues that interact with **BF** interact with the seven-carbon aliphatic chain of **HF** as it adopts a hook-like conformation (Figure 1B). The branched eight-carbon chain of the inhibitor **MHF** interacts in a more extended fashion within the hydrophobic pocket that comprises the $\gamma_2\gamma_2$

substrate-binding site. The bound conformation for **MHF** is similar to the conformation of (*R*)-*N*-1-methylhexylformamide bound within the substrate-binding site of equine liver alcohol dehydrogenase (*14*). Despite the fact that the sample of **MHF** utilized for the crystallographic experiments is a 1:1 racemic mixture (ref *13*; B. V. Plapp, personal communication), only the R-enantiomeric form of the inhibitor is observed, and the enantiomeric methyl group projects into an enlarged region of the binding pocket formed by the presence of the smaller Ser48/Val141 residues in the $\gamma_2\gamma_2$ structure (Figure 2). This same area of the substrate-binding site is also likely responsible for the enzyme's ability to oxidize 3-hydroxysteroids (*23, 24*). The most obvious structural feature of the $\alpha\alpha$ isoform is the Ala for Phe93 substitution near the catalytic zinc that enlarges the site and provides space for the disubstituted **CPCB** to bind with high complimentarity (Figure 3). As previously predicted from modeling studies (*13*), the inhibitor binds in the E-conformation with the cyclobutyl ring positioned within the hole created by the substitution of Ala for Phe93.

DISCUSSION

As previously observed, the overall structures of all three class I ADH isoenzymes are nearly identical, consistent with their ~93% sequence identity. Both the $\gamma_2\gamma_2$ and the $\beta_1\beta_1$ isoenzyme structures are of significantly higher resolution as compared to the previously published binary complexes (*9*). Despite numerous efforts, the crystals for the $\alpha\alpha$
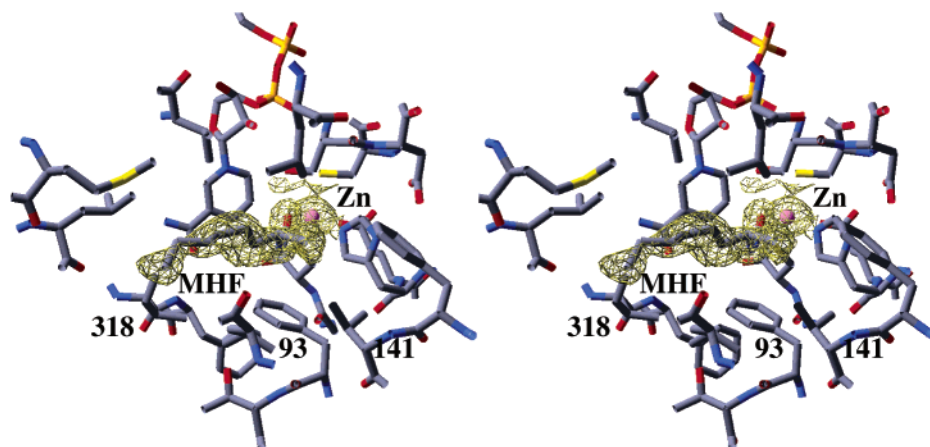
FIGURE 2: Electron density for 1-methylheptylformamide bound to human $\gamma_2\gamma_2$ alcohol dehydrogenase.
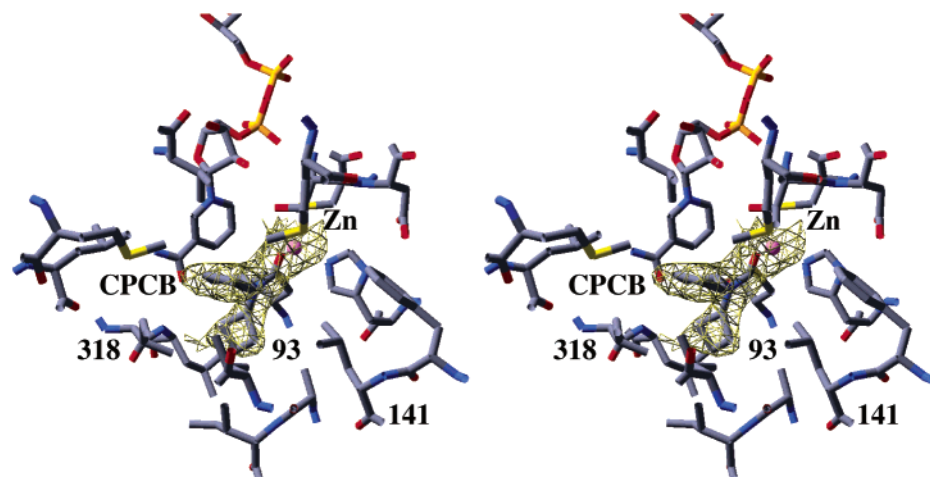

FIGURE 3: Electron density for cyclobutycyclopentylformamide bound to the human $\alpha\alpha$ alcohol dehydrogenase.

isoenzyme did not diffract significantly past the previously attained 2.5 Å. In all cases, the protein crystals were grown as binary complexes with coenzyme. Soaking the formamide inhibitor into each preexisting binary complex crystal formed the ternary complexes reported here. Aside from occupancy of the substrate-binding sites, we observe no significant changes in the structures of the individual isoenzymes relative to their previously reported structures.

The structures of the two $\beta_1\beta_1$ structures show the nature of the interactions within the binding pocket that can accommodate both aromatic and aliphatic substrates. Both **BF** and **HF** possess the same number of carbon atoms and identical binding constants (Table 1). The conformations adopted by the inhibitors while bound within the substrate-binding pockets bury very similar solvent-accessible surface areas (369 Å² **HF** vs 338 Å² **BF**). Every carbon atom of the inhibitors contacts residues within the binding pocket and therefore contributes to the overall binding energy. That **BF** is less effective as an inhibitor for the $\alpha\alpha$ and $\gamma_2\gamma_2$ isoenzymes, compared to the $\beta_1\beta_1$ isoenzyme, is likely due to steric restrictions brought about by Met57 and Val116 in the $\alpha\alpha$ isoenzyme and Ile318 in the $\gamma_2\gamma_2$ isoenzyme. Each of these residues narrows the outer region of the substrate-binding site near carbons 3−5 of the benzene ring and the entrance to the substrate-binding site (Figure 4). In the $\alpha\alpha$ isoenzyme, the loss of the amide−aromatic dipole interaction (*14*, *22*) at position 93 undoubtedly also contributes to the weaker interactions for the monosubstituted inhibitors.

Considerable work concerning the differences in substrate specificity among the human class I isoenzymes has focused on the unique characteristics of the $\alpha\alpha$ isoenzyme. In contrast to other ADH isoenzymes, the $\alpha\alpha$ isoenzyme readily oxidizes secondary alcohols with high catalytic efficiency and does so with a stereoselectivity that is opposite that of other ADH isoenzymes (*25*). This reversal of stereospecificity for secondary alcohols has been shown to result from the substitution of Ala for Phe93 (*26*). This single substitution opens up the area of the substrate pocket on the side that is opposite to that of Thr/Ser48. Not surprisingly then, the $\alpha\alpha$ isoenzyme has a very different structure−activity profile for substituted formamides. The formamide with the strongest dissociation constant was one in which two cyclized groups were attached to the amide nitrogen, **CPCB** (*13*). The structure of this compound mimics, but does not completely recapitulate, the interactions that occur with secondary alcohols or ketones since the substitution occurs at the equivalent to the C2 position of substrate alcohols or ketones. By burying its total accessible surface of 372 Å², **CPCB** effectively maps out the accessible surface of the $\alpha\alpha$ substrate-binding site, with the exception of the entry area encompassed by residues 306 and 116 (Figure 4). However, the bulk of the remaining available interactions within the substrate-binding pocket are largely hydrophilic in nature; thus, it is unlikely that the presence of an additional aliphatic substituent added to the 3-position of the cyclopentyl ring
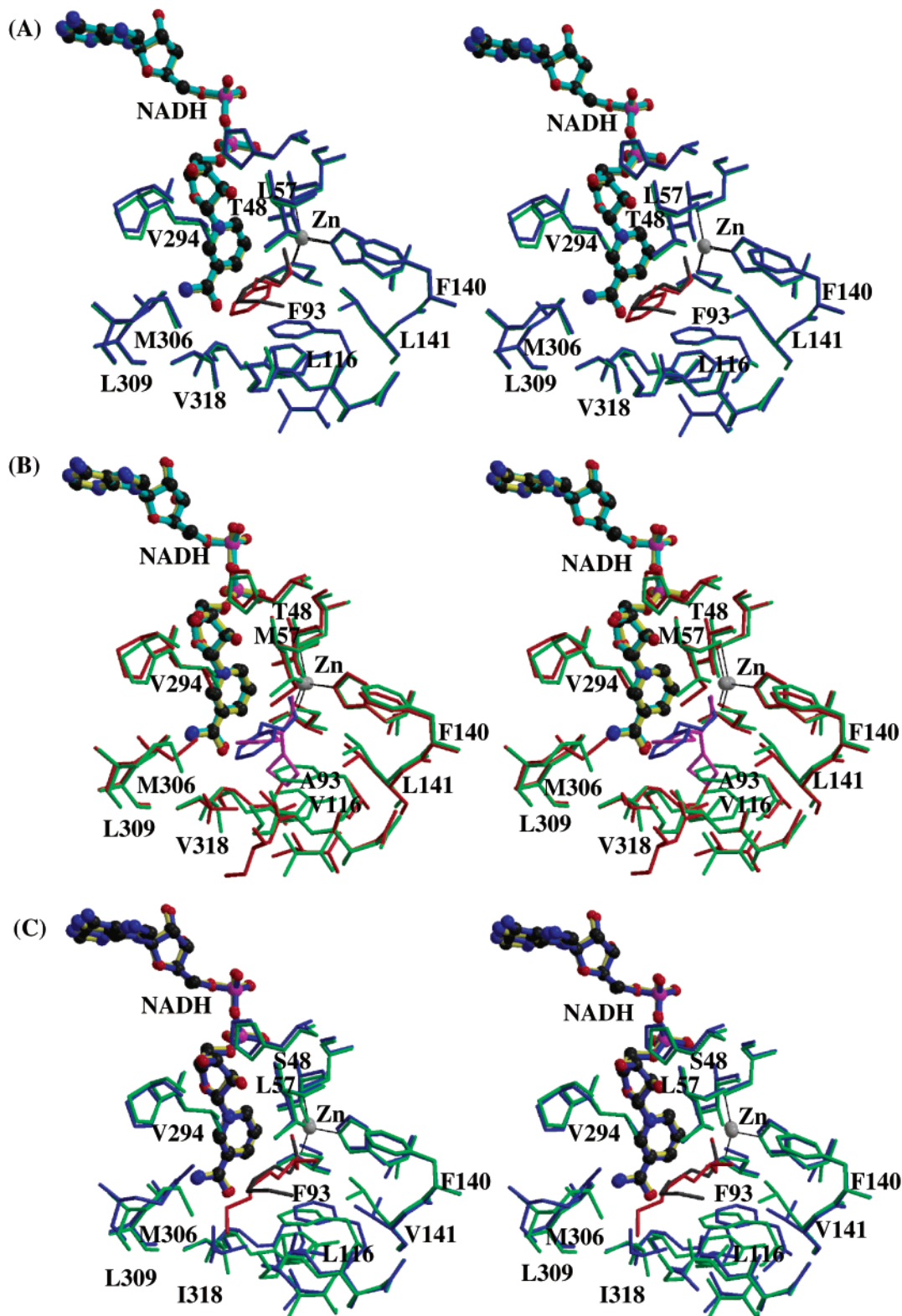
FIGURE 4: Comparison of the active site structures and the bound formamides for $\alpha\alpha$, $\beta_1\beta_1$, and $\gamma_2\gamma_2$ alcohol dehydrogenase isoenzymes. (A) An alignment of the two $\beta_1\beta_1$ structures with bound benzylformamide (red) and heptylformamide (black). (B) An alignment of the structure of $\alpha\alpha$ with bound cyclobutylcyclopentylformamide (violet) and the active site structure of the $\beta_1\beta_1$ isoenzyme. (C) An alignment of the human $\beta_1\beta_1$ and human $\gamma_2\gamma_2$ isoenzymes with their bound heptyl- (black) and 1-methylheptylformamides (red), respectively. These figures were generated using the program MOLSCRIPT (*29*) and rendered using the program RASTER3D (*30, 31*).

(*13*) would significantly enhance its interactions with the $\alpha\alpha$ isoenzyme.

   An intriguing result of this work is the enantiomeric selectivity of the $\gamma_2\gamma_2$ isoenzyme for **MHF** in comparison to the binding of the achiral **HF**. The paths of the aliphatic tails for **HF** and **MHF** are relatively similar throughout the first six atoms within the $\beta_1\beta_1$ and $\gamma_2\gamma_2$ active sites, respectively, and in both cases the final carbon of the chain is disordered as evidenced by the weak electron density at these positions (Figures 1 and 2). Thus, it is likely that the

structure of **HF** bound to the $\beta_1\beta_1$ isoenzyme would be representative of its mode of binding to the $\gamma_2\gamma_2$ isoenzyme. However, without the branched methyl substituent, **HF** would likely not completely desolvate the substrate-binding site in the vicinity of Val141. Thus, the difference in the binding constants for **HF** and **MHF** in the $\gamma_2\gamma_2$ isoenzyme undoubtedly reflects both the gain of a productive interaction with the neighboring hydrophobic residues contributed by the methyl substituent and the differences in solvation (the solvent-accessible surface area of **MHF** buried within the active site is 407 vs 369 Å^2 for **HF**). The methyl substituent at the C3 position is well-optimized for the available space at this position in the binding pocket of $\gamma_2\gamma_2$ since lengthening the substituent to an ethyl group results in a 3-fold increase in the inhibition constant (*14*). The stereoselectivity observed in this work is consistent with data using the purified enantiomers of *N*-1-methylhexylformamide, in which the purified R-enantiomer was shown to bind to the human $\gamma_2\gamma_2$ isoenzyme 7-fold more tightly than the S-enantiomer (*14*). As mentioned previously, enantiomeric selectivity is not a surprising feature of substrate binding to ADH isoenzymes. Previous work with alcohol substrates had focused on chiral differences at the C1 position of the substrate. Here, enantiomeric selectivity is achieved at the equivalent to the C3 position of a substrate, but the basis for this selectivity is the same—there is more room for chiral substituents oriented toward positions 48 and 141 in ADH isoenzymes that possess aromatic rings at position 93 (*27*).

In conclusion, the structures of the three human class I ADH isoenzymes in ternary complexes with isoenzyme specific substituted formamides provide the first substrate-level view of how the amino acid substitutions within their substrate-binding pockets give rise to their overlapping, but distinct, substrate preferences. The $\beta_1\beta_1$ isoenzyme is the most restrictive in the vicinity of the catalytic zinc atom but widens to accept both aromatic and long-chain aliphatic compounds, while both the $\gamma_2\gamma_2$ and the $\alpha\alpha$ isoenzymes have more available space for branched substituents near the catalytic zinc atom, yet are more narrow in the middle and outer regions of their respective substrate-binding sites. The $\alpha\alpha$ isoenzyme is the most unique in its substrate-binding site structure, and consequently, doubly substituted formamide compounds are the most effective inhibitors for this isoenzyme and show the greatest selectivity for this ADH isoenzyme as compared to all other known forms.

REFERENCES

1. Hurley, T. D., Edenberg, H. J., and Li, T.-K. (2002) The Pharmacogenomics of Alcoholism, in *Pharmacogenomics: The Search for Individualized Therapeutics* (Licinio, J., Wong, M.-L., Eds.) pp 417−442, Wiley-VCH, Weinheim.

2. Edenberg, H. J., and Bosron, W. F. (1997) Alcohol dehydrogenases, in *Comprehensive Toxicology, vol. 3, Biotransformation* (Guengerich, F. P., Ed.) pp 119−131, Pergamon Press, New York.

3. Yang, Z.-N., Davis, G. J., Hurley, T. D., Stone, C. L., Li, T.-K., and Bosron, W. F. (1994) Catalytic efficiency of human alcohol dehydrogenases for retinol oxidation and retinal reduction, *Alcoholism: Clin. Exp. Res. 18*, 587−591.

4. Jörnvall, H., Shafqat, J., El-Ahmed, M., Hjelmqvist, L., Persson, B., and Danielsson, O. (1996) Alcohol dehydrogenase variability: evolutionary and functional conclusions from characterization of further variants, *Adv. Exptl. Med. Biol. 414*, 281−289.

5. Edenberg, H. J. (2000) Regulation of the mammalian alcohol dehydrogenase genes, *Prog. Nucl. Acid Res. Mol. Biol. 64*, 295−341.

6. Duester, G., Farrés, J., Felder, M. R., Holmes, R. S., Höög, J.-O., Parés, X., Plapp, B. V., Yin, S.-J., and Jörnvall, H. (1999) Recommended nomenclature for the vertebrate alcohol dehydrogenase gene family, *Biochem. Pharm. 58*, 389−395.

7. Estonius, M., Svensson, S., and Höög, J.-O. (1996) Alcohol dehydrogenase in human tissues: localisation of transcripts coding for five classes of the enzyme, *FEBS Lett. 397*, 338−342.

8. Bosron, W. F., Magnes, L. J., and Li, T.-K. (1983) Kinetic and electrophoretic properties of native and recombined isoenzymes of human liver alcohol dehydrogenase, *Biochemistry 22*, 1852−1857.

9. Niederhut, M. S., Gibbons, B. J., Perez-Miller, S., and Hurley, T. D. (2001) Three-dimensional structures of the three human class I alcohol dehydrogenases, *Protein Sci. 10*, 697−706.

10. Deltour, L., Foglio, M. H., and Duester, G. (1999) Metabolic Deficiencies in alcohol dehydrogenase *Adh1*, *Adh3*, and *Adh4* null mutant mice, *J. Biol. Chem. 274*, 16796−16801.

11. Svensson, S., Stomberg, P., and Hoog, J.-O. (1999) A novel subtype of class II alcohol dehydrogenase in rodents. *J. Biol. Chem. 274*, 19712−19719.

12. Bosron, W. F., and Li, T.-K. (1987) Catalytic properties of human liver alcohol dehydrogenase isoenzymes, *Enzyme 37*, 19−28.

13. Schindler, J. F., Berst, K. B., and Plapp, B. V. (1998) Inhibition of human alcohol dehydrogenase by formamides, *J. Med. Chem. 41*, 1696−1701.

14. Venkataramaiah, T. H., and Plapp, B. V. (2003) Formamides mimic aldehydes and inhibit liver alcohol dehydrogenases and ethanol metabolism, *J. Biol. Chem. 278*, 36699−36706.

15. Xie, P. T., and Hurley, T. D. (1999) Methionine-141 directly influences the binding of 4-methylpyrazole in human $\sigma\sigma$ alcohol dehydrogenase, *Protein Sci. 8*, 2639−2644.

16. Otwinowski, Z., and Minor, W. (1997) Processing of X-ray diffraction data collected in oscillation mode, *Methods Enzymol. 276*, 307−326.

17. Collaborative Computational Project, No. 4. (1994) The CCP4 Suite: Programs for Protein Crystallography, *Acta Crystallogr. D50*, 760−763.

18. Navaza, J. (1994) AmoRe: an automated package for molecular replacement, *Acta Crystallogr. A50*, 157−163.

19. Brunger, A. T., et al. (1998) Crystallography & NMR system: A new software suite for macromolecular structure determination, *Acta Crystallogr. D54*, 905−21.

20. Murshudov, A. A., Vagin, A. A., and Dodson, E. J. (1997) Refinement of macromolecular structures by the maximum-likelihood method, *Acta Crystallogr. D53*, 240−255.

21. Jones, T. A., Cowan, S., Zou, J.-Y., and Kjeldgaard, M. (1991) Improved methods for building protein models in electron-density maps and location of errors in these models, *Acta Crystallogr. A47*, 110−119.

22. Ramaswamy, S., Scholze, M., and Plapp, B. V. (1997) Binding of formamides to liver alcohol dehydrogenase, *Biochemistry 36*, 3522−3527.

23. McEvily, A. J., Holmquist, B., Auld, D. S., and Vallee, B. L. (1988) 3β-hydroxy-5β-steroid dehydrogenase activity of human liver alcohol dehydrogenase is specific to γ-subunits, *Biochemistry 27*, 4284−4288.

24. Höög, J.-O., Eklund, H., and Jörnvall, H. (1992) A single-residue exchange gives human recombinant $\beta\beta$ alcohol dehydrogenase $\gamma\gamma$ isozyme properties, *Eur. J. Biochem. 205*, 519−526.

25. Stone, C. L., Li, T.-K., and Bosron, W. F. (1989) Stereospecific oxidation of secondary alcohols by human alcohol dehydrogenases, *J. Biol. Chem. 264*, 11112−11116.

26. Hurley, T. D., and Bosron, W. F. (1992) Human alcohol dehydrogenase: dependence of secondary alcohol oxidation on the amino acids at positions 93 and 94, *Biochem. Biophys. Res. Commun. 183*, 93−99.

27. Eklund, H., Horjales, E., Vallee, B. L., and Jörnvall, H. (1987) Computer-graphics interpretations of residue exchanges between the α, β, and γ subunits of human-liver alcohol dehydrogenase class I isoenzymes, *Eur. J. Biochem. 167*, 185−193.

28. Guex, N., and Peitsch, M. C. (1997) SWISS-MODEL and the Swiss-PdbViewer: An environment for comparative protein modeling. *Electrophoresis 18*, 2714−2723.

29. Kraulis, P. J. (1991) MOLSCRIPT: A program to produce both detailed and schematic plots of protein structures, *J. Appl. Crystallogr. 26*, 946−950

30. Merrit, E. A., and Murphy, M. E. P. (1994) Raster3D version 2.0−a program for photorealistic molecular graphics, *Acta Crystallogr. D50*, 869−873.

31. Bacon, D. J., and Anderson, W. F. (1988) A fast algorithm for rendering space-filling molecule pictures, *J. Mol. Graphics 6*, 219−220.